Title

Self-gated 4D multiphase, steady-state imaging with contrast enhancement (MUSIC) using rotating cartesian K-space (ROCK): Validation in children with congenital heart disease

Journal

Magnetic Resonance in Medicine, 78(2)

ISSN

0740-3194

Authors

Han, Fei
Zhou, Ziwu
Han, Eric
et al.

Publication Date

2017-08-01

DOI

10.1002/mrm.26376

Peer reviewed

Published in final edited form as:

Magn Reson Med. 2017 August ; 78(2): 472–483. doi:10.1002/mrm.26376.

Self-Gated 4D Multiphase, Steady-state Imaging with Contrast Enhancement (MUSIC) using Rotating Cartesian K-space (ROCK): Validation in Children with Congenital Heart Disease

Fei Han, Ph.D.[1,2], **Ziwu Zhou, B.S.**[1,2], **Eric Han**[3], **Yu Gao, B.S.**[1,4], **Kim-Lien Nguyen, M.D.**[1,5], **J. Paul Finn, M.D.**[1], and **Peng Hu, PhD**[1,4,*]

[1] Department of Radiological Sciences, David Geffen School of Medicine, University of California, Los Angeles, CA

[2] Department of Bioengineering, University of California, Los Angeles, CA

[3] Harvard Westlake School, Los Angeles, CA

[4] Biomedical Physics Inter-Departmental Graduate Program, University of California, Los Angeles, CA

[5] Division of Cardiology, VA Greater Los Angeles Healthcare System, Los Angeles, CA

Abstract

Purpose—To develop and validate a cardiac-respiratory self-gating (SG) strategy for the recently proposed multi-phase steady-state imaging with contrast enhancement (MUSIC) technique.

Methods—The proposed SG strategy uses the ROtating Cartesian K-space (ROCK) sampling, which allows for retrospective k-space binning based on motion surrogates derived from k-space center-line. The k-space bins are reconstructed using a compressed sensing algorithm. Ten pediatric patients underwent cardiac MRI for clinical reasons. The original MUSIC and 2D-CINE images were acquired as a part of the clinical protocol, followed by the ROCK-MUSIC acquisition, all under steady-state intravascular distribution of ferumoxytol. Subjective scores and image sharpness were used to compare the images of ROCK-MUSIC and original MUSIC.

Results—All scans were completed successfully without complications. The ROCK-MUSIC acquisition took 5±1 min, compared to 8±2 min for the original MUSIC. Image scores of ROCK-MUSIC were significantly better than original MUSIC at the ventricular outflow tracts (3.9±0.3 vs. 3.3±0.6, $P<0.05$). There was a strong trend towards superior image scores for ROCK-MUSIC in the other anatomic locations.

Conclusion—ROCK-MUSIC provided images of equal or superior image quality compared to original MUSIC, and this was achievable with 40% savings in scan time and without the need for physiologic signal.

* Correspondence to: Peng Hu, PhD, Department of Radiological Sciences, 300 UCLA Medical Plaza Suite B119, Los Angeles, CA 90095, penghu@mednet.ucla.edu.

Keywords

MR angiography; cardiac CINE; self-gating; pediatric congenital heart disease; motion compensation

Introduction

Contrast enhanced magnetic resonance angiography (CE-MRA) is typically performed without cardiac gating due to the time constraint imposed by breath-holding and the need to capture the first-pass of a contrast agent (1–4). This strategy is therefore very limited for evaluation of structures that are subject to cardiac motion, such as the valves, ventricular outflow tracts, cardiac chambers and the coronary arteries. To address this issue, we recently developed the four-dimensional, multiphase, steady-state imaging with contrast enhancement (MUSIC) technique, which acquires multiple high resolution 3D cardiac-phases during uninterrupted positive pressure ventilation and in the steady-state distribution phase of ferumoxytol (5). The MUSIC technique, in its current form, relies on external ECG and airway pressure signals for cardiac and respiratory motion compensation respectively. As with conventional CE-MRA, MUSIC benefits from the higher signal to noise ratio (SNR) available at high field strengths, but the ECG signal often becomes unreliable due to magneto-hydrodynamic effects at 3 Tesla (6,7) and unless patients are intubated, the airway pressure signal is not available. Therefore, an alternative cardiac and respiratory motion compensation strategy would be desirable to improve the reliability of MUSIC at high-field strengths and potentially extend the technique to patients breathing freely.

Diaphragm navigators and respiratory bellows (8–11) are often used as motion surrogates for respiratory motion compensation. However, in a 3D cine acquisition such as MUSIC, the navigator is not ideal because it interrupts the magnetization steady-state and results in a temporal window within the cardiac cycle where no imaging data are acquired. Hence, navigators are most commonly used in acquisitions that do not cover the entire cardiac cycle. Respiratory bellows are less often used because it is not a direct measurement of the underlying respiratory motion and have not been very reliable in clinical practice. Another family of technique named self-gating (SG) has been widely studied in the past decade (12–15). The SG techniques detect physiological motion directly from the k-space signal of the imaging volume, and therefore provide more direct motion estimation and gating decisions. Moreover, SG can be integrated seamlessly into most imaging sequences and allows for uninterrupted image acquisition and maintenance of the magnetization steady-state (16–18).

In this work, we sought to develop a cardiac and respiratory motion SG strategy and apply it to the MUSIC technique (5). The proposed strategy includes three components: 1) The k-space data are acquired using a “ROtating Cartesian K-space (ROCK)” trajectory, which allows variable density sampling and enables retrospective data binning; 2) The data acquired within the respiratory window are binned into multiple cardiac phases based on the cardiac and respiratory SG motion surrogates; and 3) The images are reconstructed using ESPIRiT (19), a non-linear iterative algorithm that combines compressed sensing and parallel imaging. The ROCK-MUSIC MRI technique was tested in a cohort of pediatric

patients with congenital heart disease (CHD) undergoing clinically indicated MRI with general anesthesia and positive pressure ventilation. The ROCK-MUSIC strategy was then compared with the original MUSIC MRI technique, in which the ECG and airway pressure signals were used for motion gating (5).

Method

ROCK sampling pattern

The k_y-k_z plane of the 3D Cartesian ROCK k-space grid is shown in Figure 1a, where each point represents a readout line in the k_x direction. First, all points in the plane are divided into N concentric rings. A spiral path with azimuthal angle ∅ and relative angular velocity κ=10 is generated using Eq. 1

$$\begin{cases} y(r) = r * \cos(r * \kappa + \varnothing) \\ z(r) = r * \sin(r * \kappa + \varnothing) \end{cases}, \quad r \in [0,1] \qquad \text{Eq. 1}$$

The spiral path was subsequently mapped to N Cartesian grid points along the spiral trajectory, one point from each ring. More specifically, to select a point within a k-space ring, the cost function described in Eq. 2 is minimized.

$$C_{y,z} = |\varphi_{y,z} - \varnothing| + \lambda \cdot D(y,z), \quad where \quad \varphi_{y,z} = \theta_{y,z} - r \cdot \kappa \qquad \text{Eq. 2}$$

In Eq. 2, $\varphi_{y,z}$ is the "spiral-corrected" angle of point (y, z) calculated from its azimuthal angle $\theta_{y,z}$, its radius r and the relative angular velocity κ;∅ is the azimuthal angle of the current spiral path, $D(y,z)$ is the sampling density at point (y, z), which is constantly updated. By minimizing the cost function, we choose the point that is closest to the desired spiral path while preventing any point from being sampled repetitively. After the selection of each point, the sampling density matrix is updated by convoluting the selected points with a 5×5 Gaussian kernel, which not only prevents a point from being sampled too frequently, but also avoids local clustering of sampling points. Conventional receiver coil arrays could support 2X to 3X under-sampling in each direction and the missing samples are recovered by parallel imaging, which is the main reason that a similar sized Gaussian kernel was used, although the specific size and shape of the kernel was chosen empirically. The entire process is then repeated for each spiral trajectory with the ∅ incremented using the segmented golden ratio (20), until the desired number of samples is reached.

In this study, the Cartesian grid was divided into N=20 rings and the area of each ring grew exponentially from the most inside one to the outside ones. In this way, the final sampling pattern had variable sampling density (21) where the center k-space was sampled more often than the peripheral, because equal number of sampling points were chosen from each rings. Moreover, the most inside ring had only one point in the center, which was therefore sampled once in every quasi-spiral path and subsequently used for SG. In addition, each quasi-spiral path was a "spiral-in" trajectory rather than "spiral-out" in order to minimize the interference of the eddy current effects on the SG signal. As shown in **Figure 1**(b), with the

"spiral-out" trajectory, the SG line at the beginning of a quasi-spiral path is immediately preceded by a peripheral k-space line at the end of the previous quasi-spiral path. The large phase-encoding gradients during the acquisition of the peripheral k-space line could cause distortion of the SG signal due to eddy current effects, a problem reported in several previous SG methods (18,22,23). With the "spiral-in" trajectory, the SG line had less distortion and the motion estimations were more reliable. This is because they were preceded by k-space lines in the center region with much smaller phase-encoding gradients and therefore has less eddy current effects.

The algorithm was implemented based on a 3D gradient-recalled-echo (GRE) sequence to generate the ROCK pattern on the fly for different matrix sizes and under-sampling rates, typically within 5 seconds after the pulse sequence parameters are set. The sequence acquires k-space data continuously and is not synchronized with either cardiac or respiratory motion. The total acquisition time is calculated based on matrix size, estimated respiratory gating efficiency (40%) and TR in order to achieve a user-defined desirable under-sampling rate for each cardiac phase after data binning.

Motion Estimation and Data Binning

The SG lines in each quasi-spiral arm of the ROCK pattern were used to generate motion surrogates. They were first Fourier transformed into projections in the superior inferior (SI) direction and then interpolated 8-fold in order to improve the spatial definition of the projection lines as well as the subsequent motion estimates, and offer more motion weights with smoother changes in the soft-gated image reconstruction. The displacement of the current SI projection relative to the reference (i.e. first SI projection) was estimated by maximizing the cross-correlation in Eq. 3 and used as the respiratory surrogate signal. In Eq., $\mathbf{f_t}$ is the current SI projection vector shifted by t and $\boldsymbol{g}$ is the reference projection vector; $\overline{\mathrm{f_t}}$ and $\bar{g}$ are the average of $\mathbf{f_t}$ and $\boldsymbol{g}$, respectively; $\boldsymbol{\sigma}$ represents the standard deviation. Compared with using cross-correlation coefficient directly (17,18,22), this method calculates respiratory motion in millimeters and is not sensitive to the choice of reference. Furthermore, each SI projection was concatenated with its temporal neighbors (T=3) for cross-correlation calculation, which, based on our experience, effectively suppressed the cardiac motion. The cardiac motion surrogate was calculated separately as the center-of-mass of the SI projection processed by a band-pass filter with 5hz bandwidth centered at the patient's heart beat frequency (24).

$$\mathrm{d} \quad = \quad \mathrm{argmax}_{\mathrm{t}\in\mathbb{R}} \frac{\sum_{\mathrm{x}} \left[\left(\mathrm{f_t} - \overline{\mathrm{f_t}} \right) \cdot \left(\mathrm{g} - \bar{\mathrm{g}} \right) \right]}{\sigma_{\mathrm{f_t}} \cdot \sigma_{\mathrm{g}}} \qquad \text{Eq.3}$$

Motion compensation was performed on all acquired k-space data using the derived SG motion surrogates. The cardiac motion signal first underwent peak detection to identify the triggers for each heartbeat and the ones with abnormal duration (i.e. beyond one standard deviation from the average duration of all heartbeats) are discarded. Then, each remaining heartbeat is evenly divided into 9 cardiac phases and the corresponding k-space data were

sorted accordingly for each cardiac phase. For respiratory motion, a soft-gating method was applied which generates Gaussian shaped weightings based on the SG signal rather than a binary mask in traditional gating methods (25). The Gaussian kernel has a Full Width Half Max (FWHM) of 3mm and was place so that it covers the largest area in the respiratory motion histogram, which is usually the end expiration position. An example of the motion compensation process is illustrated in **Figure 2**.

Image Reconstruction

After motion compensation, the k-space data of each cardiac phase are reconstructed using Eq.4, where ***x*** is the reconstructed volumetric image, ***D*** and **F** represent under-sampling and Fourier transform operations, ***S*** is the sensitivity maps of all the receiver coils estimated using ESPIRiT method (19), **y** is the under-sampled k-space measurement from each receiver coils, ***w*** is the soft-gating term calculated from the derived respiratory SG motion surrogate, Ψ(x) is the regularization term on spatial sparsity in the wavelet domain.

$$\mathrm{f}(\mathbf{x}) \quad = \quad \mathrm{argmin}_{\mathbf{x}} \| \, \mathbf{w} \, (\mathbf{D} \mathscr{F} \mathbf{S}_{\mathbf{x}} - \mathbf{y}) \, \|_2^2 \quad + \quad \lambda \Psi \, (\mathbf{x}) \qquad \text{Eq.4}$$

Motion compensation and image reconstruction algorithms were implemented in a custom-built PC (quad-core CPU, 32GB memory) with parallelized GPU acceleration using C++ and the BART toolbox (26). The PC was connected with the MRI scanner via Ethernet cable so that k-space data are transferred to the PC as they are acquired and images are sent back to the scanner upon the completion of reconstruction (27). A graphical interface was also developed that allows the user to input parameters (e.g. patient's heart rate, size and shape of the respiratory gating window etc.) and monitor the progress as well as the intermediate results of the reconstruction process. Our implementation allows the image reconstruction to be performed in minutes and fully integrated into the current clinical workflow.

Phantom Experiments

Phantom experiments were performed to evaluate the proposed ROCK sampling pattern. Scan parameters were set to match approximately those to be used in clinical scans (1.2ms/2.9ms, matrix size: 480×280×140, 1mm^3 isotropic resolution, scan time=5min). A pair of scans were first performed to compare SG signal using the "spiral-in" and "spiral-out" ROCK sampling. The data using the "spiral-in" ROCK were retrospectively gated to end-expiration and binned into 9 cardiac phases using a recorded physiological signal from a previously scanned pediatric patient whose average heart rate was 118bpm. Standard 3D GRE scans with identical matrix size and resolution settings were performed using 2×2 and 3×2 GRAPPA in the ky-kz acceleration, resulting in a net acceleration factor of 3.7× and 5.4×, respectively. The data using GRAPPA sampling were reconstructed using the vendor-provided software and the data using ROCK sampling reconstructed offline using Eq.4. The experiments were performed on 1.5T and 3T scanners (Magnetom TIM Avanto/Prisma, Siemens Medical Solutions).

In-vivo Experiments

The in-vivo study was approved by our institutional review board. Ten pediatric patients with complex congenital heart disease (CHD) who were referred for clinical cardiovascular MRI independent of our research (ages 1 month to 8 years, 5 males) were included in this study. Ferumoxytol was administrated as an MRI contrast agent at an elemental iron dose of 4mg/kg body weight by slow infusion. The patients were under general anesthesia at the time of MRI, which is our institutional standard practice for young patients who cannot reliably follow verbal instructions during scanning. The patients were monitored by pediatric anesthesiologists throughout the MRI examination. All imaging was done on a 3.0T scanner (Magnetom TIM Trio, Siemens Medical solutions). Receiver coils, including adult knee coil, head coil, flex coil, or body array coil were configured for specific patient size to provide optimal coverage.

The approved institutional protocol for these patients included the original MUSIC with ECG and ventilator gating and 2D CINEs using ventilator controlled breath-holding. The ROCK MUSIC acquisition was performed with scan parameters matching those of the original MUSIC: 1.2ms/2.9ms, matrix size: 480×280×140, 0.8-1mm^3 isotropic resolution, 9 cardiac phases FA=20°. Parameters of the 2D CINE scans included: GRE readout, 1.7/4.1ms, FA=20°, 1mm in-plane resolution, 4mm slice thickness, 40-60ms temporal resolution. As the intravascular half-life of ferumoxytol is approximately 15 hours, the blood concentration was effectively constant throughout the entire study. The original MUSIC parameters were set to achieve 2.8X acceleration with an acquisition time of 7-9min. The acquisition time of the ROCK-MUSIC was set to 60% of the original MUSIC with 5X acceleration (TA=4-6min). Physiologic signals, including airway pressure and ECG, were recorded in all cases. Image reconstruction was initiated automatically after data acquisition and all 4D DICOM images were ready for review at the scanner console within 10 minutes, without interrupting intervening image acquisition (as for 2D cine). To compare the performance of the conventional binary respiratory gating strategy with our soft-gating, retrospective image reconstruction was performed based on one ROCK-MUSIC dataset using the conventional binary respiratory gating strategy. The binary gating window was placed at the same position as the soft-gating kernel, with window width of 3mm, which was identical to the FWHM of the soft-gating kernel.

Data Analysis

The respiratory SG signal was correlated with the recorded airway pressure signal for each subject. The cardiac SG triggers were validated against the recorded ECG triggers, and the standard deviation of the difference between SG and ECG trigger times were calculated. Similar methods were used in previous SG studies (24,28,29).

Visual assessment of the subjective image quality of both techniques was performed by a board-certified physician with >5 years of experience in cardiovascular MRI. The images of the original MUSIC and ROCK-MUSIC were presented in random order to the evaluator, who was blinded to the patient information and the imaging technique. Image quality scores were recorded for four anatomic structures, using criteria listed in Table 1.

Image sharpness was measured in the left ventricle and diaphragm by drawing a linear profile and calculating the slope of the signal density, as previously described (5). The slopes on both sides were defined as the image intensity difference divided by the distance between the two points at 20% and 80% of the dynamic range, respectively. The calculated slope on both sides was then averaged as the final sharpness measurement.

The end systolic volume (ESV) and end diastolic volume (EDV) of the left and right ventricle (LV/RV) were measured based on the original MUSIC and the ROCK-MUSIC images. The 4D images are first reformatted to stacks of 2D slices in the standard short-axis view. The endomyocardial borders of the original MUSIC and ROCK-MUSIC datasets were manually drawn for each 2D slice using an OsiriX workstation and the volumes were calculated by integrating the results for all the 2D slices.

The subjective image quality scores were compared using the Wilcoxon signed-rank test. Vessel sharpness measurements were compared using paired student t-test. $P<0.05$ is considered statistically significant. The ventricular volume measurements were compared using Bland-Altman analysis.

Result

Phantom Experiments

Figure 3a-b shows the projections of a static phantom in 1.5T using ROCK pattern with spiral-out and spiral-in sampling, respectively. Fluctuations of the projection magnitudes over time due to eddy current are apparent in the spiral-out case because the acquisition of the SG line is immediately preceded by a peripheral k-space line with strong gradients in the previous quasi-spiral interleaf. These fluctuations are much reduced in the spiral-in projections because the same SG line acquisition is preceded by an adjacent line in the center k-space region.

The images reconstructed from the ROCK under-sampled data in both 1.5T (Figure 3c) and 3T (Figure 3d) are free of the aliasing artifacts that are often seen in the ones reconstructed from GRAPPA under-sampled data, even though higher under-sampling rate was achieved. Figure 3c-d also shows the k-space sampling pattern of the first and last cardiac phases. The segmented golden ratio increment of the quasi-spiral paths in ROCK ensures a near-uniform angular distributions of the k-space samples after retrospective motion gating and data binning (20).

In-vivo Experiments

All clinical scans were completed successfully. The image reconstruction time among all the subjects was 6.4±0.9 minutes for a complete 4D dataset. Figure 4 shows a section of the SI projections along with the calculated respiratory self-gating (RSG) and cardiac self-gating (CSG) signal from a 19 month-old, male subject compared to the recorded air-pressure signal and the ECG trigger. The RSG correlates well with the recorded air-pressure signal. The cardiac triggers detected from the CSG also matched with the recorded ECG triggers albeit with a small delay. The delay may be explained by the time difference between the electrical stimulus and the actual mechanical motion, as the CSG signal is a direct

measurement of the actual motion. For all subjects, the averaged correlation coefficient between RSG and airway pressure was 0.94±0.025. The averaged standard deviation of the time difference between CSG and ECG triggers was 12.96±3.71ms. The heart rate based on ECG signal was 106.3±12.4 bpm and the ones based on self-gating signal was 104.9±11.6 bpm. Three patients with poor ECG signal despite multiple attempts to replace the ECG electrodes were excluded in this comparison.

Figure 5 shows single frame images (1mm slice thickness, no Maximum-Intensity-Projection) of the original MUSIC and ROCK-MUSIC from a 6-years-old female patient (2 of 9 cardiac phases are shown). ROCK-MUSIC provides images of equal quality, if not superior, to the original MUSIC, and this is achievable with a 40% reduction in scan time and without the need for physiologic signal. Movie versions of Figure 5 are available as Supporting Video S1 and S2 in the Online Supplemental Materials. Figure 6 shows images from an 8-year-old male whose ECG signal was unstable during the scan. The blood-myocardium border is blurred due to inaccurate cardiac triggering in the images reconstructed based on ECG (Figure 6b). Conversely, images which were reconstructed from the same k-space data but used cardiac SG triggers show less motion artifacts and have better image quality in the regions which are subject to cardiac motion.

A comparison of conventional respiratory binary gating and soft-gating based on one volunteer dataset is presented in Supporting Figure S1 in the Online Supplemental Materials. The blood-pool SNR of soft-gating reconstruction was 35% higher than the binary gating reconstruction (29.7 vs. 21.9). The diaphragm border of soft-gating reconstruction was also sharper than the binary gating reconstruction (0.28 vs. 0.25).

As shown in Table 2, image scores of ROCK-MUSIC were significantly better than original MUSIC at the ventricular outflow tracts (3.9±0.3 vs. 3.3±0.6, $P<0.05$). In the other three anatomic locations evaluated, there was a strong trend towards superior image scores for ROCK-MUSIC, although the comparison was not statistically significant. Quantitative image sharpness between ROCK-MUSIC and original MUSIC were comparable (0.29±0.18 vs. 0.28±0.15 for the LV, and 0.30±0.13 vs. 0.28±0.11 for the diaphragm, $P>0.05$). The Bland-Altman plots of ventricular volume measurement based on the original MUSIC and ROCK-MUSIC is shown in Supporting Figure S2. The bias of LV volume measurements based on the two techniques was 0.31cm^3, with 95% confidential interval (CI) [−0.26 0.88] cm^3. The bias of RV volume was 0.2 cm^3, with 95% CI [−0.38 0.78] cm^3. The ventricular volume measurements among the subjects had relatively large variance because of the wide age range (0-6 years old) and size of the patients.

The isotropic resolution (<1mm^3), motion compensated, high quality 4D images offered by ROCK-MUSIC allows retrospective 2D reformatting in arbitrary orientations and in multiple cardiac phases to facilitate interrogation of detailed intra-cardiac and vascular structures. Figure 7 shows reformatted 2D short axis images with image quality that is comparable to that of 2D cardiac CINE using ventilator controlled breath-held and ECG gating. The volumetric excitation of 4D ROCK-MUSIC is free of blood in-flow de-phasing artifacts that are sometimes associated with 2D CINE acquisitions and results in a more homogeneous blood-pool signal, which is potentially beneficial for automated blood-pool segmentation.

Further, ROCK-MUSIC allows for multi-phase visualization of major coronary arteries even in very small children, as shown in Figure 8.

Discussion

The current work represents a feasibility study of the self-gated ROCK-MUSIC in pediatric CHD patients. Our results show that, in a small cohort of children with complex CHD, the self-gated ROCK-MUSIC technique produced image quality at least as good as the original 4D MUSIC acquisition without the need for external respiratory or cardiac signals and with a 40% reduction in imaging time. The patients in our study were under general anesthesia with positive pressure ventilation, which provides an excellent reference standard against which to validate our motion self-gating signal. Therefore, the development and validation of our ROCK-MUSIC technique is an important step towards generalizing our ferumoxytol-enhanced 4D MRI to older CHD patients who undergo cardiovascular MRI during free breathing without anesthesia.

Several technical components of the proposed methods have contributed to the overall improvement over original MUSIC in terms of image quality and acquisition speed. First, the cardiac and respiratory SG signals enabled more accurate and reliable motion gating decisions. We experienced ECG signal distortions due to interference in 3 subjects in this study, which resulted in false and missing cardiac triggers during MUSIC acquisition. In these cases, the SG triggers in ROCK-MUSIC could better represent the true cardiac motion because the signal is not affected by the magnet and gradient systems. Second, the variable density quasi-random ROCK sampling and ESPIRiT (19) image reconstruction in ROCK-MUSIC is more efficient than conventional structurally under-sampled Cartesian sampling and GRAPPA used in the original MUSIC. The ESPIRiT algorithm uses an eigenvalue approach to better estimate the coil sensitivity map and a spatial wavelet regularization term was integrated in the image reconstruction formula to remove the noise-like under-sampling artifacts in the images.

The retrospective nature of the proposed motion self-gating method provides several advantages over prospective methods (28,30). First, the respiratory gating window and position are defined after the image acquisition. Respiratory drift, which is one of the major challenges in prospective methods (30), can be addressed in retrospective methods by analyzing the respiratory motion histogram and choosing the gating window and position for maximized gating efficiency. Moreover, retrospective cardiac triggering allows for complete coverage of all cardiac phases whereas images during the 40-80ms triggering window is not available in prospective cardiac triggering methods. This is particularly important for the pediatric CHD application because these young children typically have high heart rates of 120-140bpm and 40-80ms represents a significant portion of the cardiac cycle.

Many previously proposed retrospective motion compensation techniques were based on radial sampling. Despite the benefits including straight-forward combination with golden-angle schemes and relative immunity to motion artifacts, radial sampling is associated with limitations in clinical practice (14,31). First, the sampling efficiency of radial sampling is compromised when anisotropic fields-of-view are preferred. In addition, radial sampling

requires computationally intensive reconstruction, which is non-trivial especially when non-linear iterative methods are used. Even when modern computing technology such as parallelized GPU acceleration is incorporated, computational challenges remain. Instead, the proposed method is based on Cartesian sampling, which offers flexible fields-of-view settings that can be tailored to individual subjects for more efficient image acquisition. Moreover, 4D image reconstruction is finished within 10 minutes after scan completion and the entire process has been integrated within our current institutional clinical work flow for imaging pediatric CHD patients. On the other hand, reconstruction of radial data of a similar size would require multiple hours using comparable hardware and software implementation (31).

As the quasi-spiral interleaves traverse quickly between the center and periphery of the k-space, it is important to use a spiral-in trajectory to reduce eddy current effects from the phase-encoding gradients of the SG k-space line. Previous studies have also noted the problems of eddy currents and their effect on the reliability of motion self-gating signals (18,22,23). Deng et al.(22) proposed a solution, which acquires multiple SG lines and uses the last line to minimize eddy currents at the cost of extended acquisition time. In the ROCK pattern, we use the spiral-in sampling to address this problem. For ethical reasons, we did not make direct comparisons between the technique proposed by Deng et al. and the ROCK pattern in our patient scans. However, two findings from our study support our conclusion that the spiral-in ROCK k-space sampling provides reliable SG signal and minimize eddy current effects: 1) projection images from static phantom experiments in Figure 4 are highly reproducible and 2) the derived SG signal matched well with the recorded physiologic signal.

Golden-ratio k-space sampling is widely used in many dynamic MR imaging applications because it offers near uniform k-space sampling within any single temporal window. However, the sampling uniformity is no longer supported when golden ratio is applied in respiratory and cardiac motion gating applications. In these applications, the k-space data are selected from several temporally isolated windows (e.g. end-expiration or certain cardiac phase) instead of a single one (20,32). As a result, the k-space sampling pattern after retrospective motion gating may not be as uniform as the one using a single reconstruction window. To address this issue, segmented golden ratio (20) was used in the proposed ROCK method in which the k-space is first divided into multiple segments. Golden-ratio sampling is performed within each segment and different segments are switched in a pseudo-random order. The added degree of randomness ensures a much uniform k-space sampling pattern after retrospective data binning (33).

In the proposed methods, the data consistency term in the image reconstruction equation was weighted with the respiratory motion position. Data acquired at the center of the gating window were given larger weights and therefore likely to remain unchanged. Data acquired further away from the gating window were given weights close to 0 and therefore more likely to be updated during the optimization. This k-space weighted, or “soft-gated”, image reconstruction has been used in several recent thoracic and abdominal MR imaging applications to weight data with imperfections (e.g. motion) (25,34). Compared with the traditional binary-gating method, more data are included into the image reconstruction

framework. Meanwhile, k-space data acquired outside the traditional gating window is given less weights in the data consistency term in order to minimize the potential motion artifacts associated with including more data into the reconstruction. Cheng et al. reported an increase in SNR and image sharpness by using soft-gating in contrast-enhanced 4D phase-contrast imaging application (35). Furthermore, the use of soft-gating does not further increase the computational complexity compared with compressed sensing using binary-gating.

In the proposed method, the respiratory motion surrogate was calculated from SI projections, which includes signals from the entire excitation volume. Therefore, signals from static tissue, including chest wall and subcutaneous fat may potentially impair the accuracy of the derived motion displacement, a problem recognized in several previous studies (36). However, we did not find it problematic in our study mostly because the intravascular contrast agent, ferumoxytol, provided a uniform and stable blood-pool enhancement that contributed to the majority of the SI projection. The signal from subcutaneous fat was also much less significant than the blood-pool signal especially in these young children.

The ROCK-MUSIC could provide high-quality dynamic information of the heart in $<1mm^3$ isotropic resolution and without the need of repeated breath-held. In addition, the ROCK-MUSIC images have uniform blood-pool signal that is free of the intra-voxel dephasing artifacts usually caused by turbulent flow in conventional 2D CINE images. This is because the optimized short TE of 1.2ms and the voxel size that is 5-10 folds smaller than conventional 2D CINE. These properties support the potential of automatic 3D blood-pool segmentation and cardiac functional assessment based on the ROCK-MUSIC images. Our current protocol has limited number of cardiac phase compared with conventional 2D CINE, which has prevented the ROCK-MUSIC from reaching its full potential in cardiac functional assessment. It is the goal of our ongoing work to further improve the temporal resolution of the ROCK-MUSIC using advanced temporal acceleration methods so that it can replace conventional 2D CINE in these exams. The k-space sampling pattern of ROCK-MUSIC is not identical among the cardiac phases because the retrospective binning was performed over data acquired over 600 heart beats without cardiac motion synchronization. Such non-coherent temporal sampling could better support image reconstruction that exploits the temporal correlation of the dataset (37,38).

In this work, the use of ferumoxytol as an intravascular contrast agent greatly improved the blood-myocardium contrast in our ROCK-MUSIC images. However, ferumoxytol administration is also associated with potentially adverse events including anaphylactic reactions, which is highlighted by the FDA boxed warning in March 2015. As the CHD patients referred for MRI are typically patients who have already undergone inconclusive or insufficient echocardiography exam, ferumoxytol use in these patients may be clinically justified, especially in light of recent discovery of gadolinium deposition in human tissues after exposure to gadolinium-base contrast agents (39–41). At our institution, ferumoxytol-enhanced MRI has become our local clinical standard for MRI of pediatric CHD patients and personnel who are trained to handle any adverse reactions were immediate available throughout the MRI exam for every patient.

Conclusion

ROCK-MUSIC acquisition provided images of equal and in some anatomic locations, superior image quality, compared to original MUSIC, and this was achievable with 40% savings in scan time and without the need for physiologic signal. The proposed ROCK-MUSIC could potentially enable a more general application of the ROCK-MUSIC technique in older children and adults with CHD who do not require anesthesia for MRI.

Supplementary Material

Refer to Web version on PubMed Central for supplementary material.

Acknowledgement

The authors acknowledge research support from National Institutes of Health (1R01127153).

Reference

1. Ntsinjana HN, Hughes ML, Taylor AM. The Role of Cardiovascular Magnetic Resonance in Pediatric Congenital Heart Disease. J. Cardiovasc. Magn. Reson. 2011; 13:51. [PubMed: 21936913]
2. Prince MR, Meaney JFM. Expanding role of MR angiography in clinical practice. Eur. Radiol. 2006; 16(Suppl 2):B3–8. [PubMed: 16802437]
3. Nguyen K-L, Khan SN, Moriarty JM, Mohajer K, Renella P, Satou G, Ayad I, Patel S, Boechat MI, Finn JP. High-field MR imaging in pediatric congenital heart disease: Initial results. Pediatr. Radiol. 2015; 45:42–54. [PubMed: 25086500]
4. Saleh RS, Patel S, Lee MH, Boechat MI, Ratib O, Saraiva CR, Finn JP. Contrast-enhanced MR angiography of the chest and abdomen with use of controlled apnea in children. Radiology. 2007; 243:837–46. [PubMed: 17517937]
5. Han F, Rapacchi S, Khan S, Ayad I, Salusky I, Gabriel S, Plotnik A, Finn JP, Hu P. Four-dimensional, multiphase, steady-state imaging with contrast enhancement (MUSIC) in the heart: A feasibility study in children. Magn. Reson. Med. 2015; 74:1042–1049. [PubMed: 25302932]
6. Fischer SE, Wickline SA, Lorenz CH. Novel real-time R-wave detection algorithm based on the vectorcardiogram for accurate gated magnetic resonance acquisitions. Magn. Reson. Med. 1999; 42:361–70. [PubMed: 10440961]
7. Dimick RN, Hedlund LW, Herfkens RJ, Fram EK, Utz J. Optimizing electrocardiograph electrode placement for cardiac-gated magnetic resonance imaging. Invest. Radiol. 1987; 22:17–22. [PubMed: 3818232]
8. Ehman RL, McNamara MT, Pallack M, Hricak H, Higgins CB. Magnetic resonance imaging with respiratory gating: techniques and advantages. AJR. Am. J. Roentgenol. 1984; 143:1175–82. [PubMed: 6333787]
9. Santelli C, Nezafat R, Goddu B, Manning WJ, Smink J, Kozerke S, Peters DC. Respiratory bellows revisited for motion compensation: preliminary experience for cardiovascular MR. Magn. Reson. Med. 2011; 65:1097–102. [PubMed: 21413074]
10. Wang Y, Rossman PJ, Grimm RC, Riederer SJ, Ehman RL. Navigator-echo-based real-time respiratory gating and triggering for reduction of respiration effects in three-dimensional coronary MR angiography. Radiology. 1996; 198:55–60. [PubMed: 8539406]
11. Stuber M, Botnar RM, Danias PG, Kissinger KV, Manning WJ. Submillimeter three-dimensional coronary MR angiography with real-time navigator correction: comparison of navigator locations. Radiology. 1999; 212:579–87. [PubMed: 10429721]
12. Larson AC, White RD, Laub G, McVeigh ER, Li D, Simonetti OP. Self-gated cardiac cine MRI. Magn. Reson. Med. 2004; 51:93–102. [PubMed: 14705049]

13. Larson AC, Kellman P, Arai A, Hirsch GA, McVeigh E, Li D, Simonetti OP. Preliminary investigation of respiratory self-gating for free-breathing segmented cine MRI. Magn. Reson. Med. 2005; 53:159–68. [PubMed: 15690515]
14. Cheng JY, Zhang T, Ruangwattanapaisarn N, Alley MT, Uecker M, Pauly JM, Lustig M, Vasanawala SS. Free-breathing pediatric MRI with nonrigid motion correction and acceleration. J. Magn. Reson. Imaging. 2015; 42:407–420. [PubMed: 25329325]
15. Piccini D, Littmann A, Nielles-Vallespin S, Zenge MO. Respiratory self-navigation for whole-heart bright-blood coronary MRI: methods for robust isolation and automatic segmentation of the blood pool. Magn. Reson. Med. 2012; 68:571–9. [PubMed: 22213169]
16. Forman C, Piccini D, Grimm R, Hutter J, Hornegger J, Zenge MO. High-resolution 3D whole-heart coronary MRA: a study on the combination of data acquisition in multiple breath-holds and 1D residual respiratory motion compensation. MAGMA. 2014; 27:435–443. [PubMed: 24402560]
17. Hu P, Hong S, Moghari MH, Goddu B, Goepfert L, Kissinger KV, Hauser TH, Manning WJ, Nezafat R. Motion correction using coil arrays (MOCCA) for free-breathing cardiac cine MRI. Magn. Reson. Med. 2011; 66:467–75. [PubMed: 21773986]
18. Pang J, Bhat H, Sharif B, Fan Z, Thomson LEJ, LaBounty T, Friedman JD, Min J, Berman DS, Li D. Whole-heart coronary MRA with 100% respiratory gating efficiency: self-navigated three-dimensional retrospective image-based motion correction (TRIM). Magn. Reson. Med. 2014; 71:67–74. [PubMed: 23401157]
19. Uecker M, Lai P, Murphy MJ, Virtue P, Elad M, Pauly JM, Vasanawala SS, Lustig M. ESPIRiT-an eigenvalue approach to autocalibrating parallel MRI: Where SENSE meets GRAPPA. Magn. Reson. Med. 2013; 1001:990–1001.
20. Han F, Zhou Z, Rapacchi S, Nguyen KL, Finn JP, Hu P. Segmented golden ratio radial reordering with variable temporal resolution for dynamic cardiac MRI. Magn. Reson. Med. 2016; 76:94–103. [PubMed: 26243442]
21. Lustig M, Donoho D, Pauly JM. Sparse MRI: The application of compressed sensing for rapid MR imaging. Magn. Reson. Med. 2007; 58:1182–95. [PubMed: 17969013]
22. Deng Z, Pang J, Yang W, Yue Y, Sharif B, Tuli R, Li D, Fraass B, Fan Z. Four-dimensional MRI using three-dimensional radial sampling with respiratory self-gating to characterize temporal phase-resolved respiratory motion in the abdomen. Magn. Reson. Med. 2016; 75(4):1574–85. [PubMed: 25981762]
23. Han F, Rapacchi S, Hu P. Improved cardiac motion self-gating. J. Cardiovasc. Magn. Reson. 2013; 15(Suppl 1):P83.
24. Pang J, Sharif B, Fan Z, Bi X, Arsanjani R, Berman DS, Li D. ECG and navigator-free four-dimensional whole-heart coronary MRA for simultaneous visualization of cardiac anatomy and function. Magn. Reson. Med. 2014; 72:1208–1217. [PubMed: 25216287]
25. Forman C, Piccini D, Grimm R, Hutter J, Hornegger J, Zenge MO. Reduction of respiratory motion artifacts for free-breathing whole-heart coronary MRA by weighted iterative reconstruction. Magn. Reson. Med. 2015; 73:1885–1895. [PubMed: 24912763]
26. Uecker, Martin, Ong, Frank, Tamir, Jonathan I., Bahri, Dara, Virtue, Patrick, Cheng, Joseph Y., Zhang, Tao. Berkeley Advanced Reconstruction Toolbox; ISMRM 23rd Scientific Session; Toronto, Canada. 2015. p. 2486ML
27. Han, F., Zhou, Z., Sung, K-H., Finn, JP., Hu, P. A low-cost, Clinical Friendly Non-Linear Parallized MR Image Reconstruction Framework: Initial Proof of Concept on Pediatric Contrast Enhanced MRA Application; ISMRM 23rd Scientific Session; Toronto, Canada. 2015.
28. Buehrer M, Curcic J, Boesiger P, Kozerke S. Prospective self-gating for simultaneous compensation of cardiac and respiratory motion. Magn. Reson. Med. 2008; 60:683–690. [PubMed: 18727084]
29. Ingle RR, Santos JM, Overall WR, McConnell MV, Hu BS, Nishimura DG. Self-gated fat-suppressed cardiac cine MRI. Magn. Reson. Med. 2015; 73:1764–74. [PubMed: 24806049]
30. Xie Y, Fan Z, Saouaf R, Natsuaki Y, Laub G, Li D. Adaptive online self-gating (ADIOS) for free-breathing noncontrast renal MR angiography. Magn. Reson. Med. 2015; 73(1):312–7. [PubMed: 24478221]

31. Feng L, Grimm R, Tobias Block K, Chandarana H, Kim S, Xu J, Axel L, Sodickson DK, Otazo R. Golden-angle radial sparse parallel MRI: Combination of compressed sensing, parallel imaging, and golden-angle radial sampling for fast and flexible dynamic volumetric MRI. Magn. Reson. Med. 2013; 72:707–717. [PubMed: 24142845]
32. Kawaji K, Foppa M, Roujol S, Akçakaya M, Nezafat R. Whole heart coronary imaging with flexible acquisition window and trigger delay. PLoS One. 2015; 10(2):e0112020. [PubMed: 25719750]
33. Han F, Zhou Z, Han ES, Finn J, Hu P. Cardiac and respiratory self-gated 4D multi-phase steady-state imaging with ferumoxytol contrast (MUSIC). J. Cardiovasc. Magn. Reson. 2016; 18(Suppl 1):O51.
34. Johnson KM, Block WF, Reeder SB, Samsonov A. Improved least squares MR image reconstruction using estimates of k-space data consistency. Magn. Reson. Med. 2012; 67:1600–8. [PubMed: 22135155]
35. Cheng JY, Hanneman K, Zhang T, Alley MT, Lai P, Tamir JI, Uecker M, Pauly JM, Lustig M, Vasanawala SS. Comprehensive motion-compensated highly accelerated 4D flow MRI with ferumoxytol enhancement for pediatric congenital heart disease. J. Magn. Reson. Imaging. 2016; 43(6):1355–68. [PubMed: 26646061]
36. Lai P, Larson AC, Park J, Carr JC, Li D. Respiratory self-gated four-dimensional coronary MR angiography: A feasibility study. Magn. Reson. Med. 2008; 59:1378–1385. [PubMed: 18506786]
37. Tsao J, Boesiger P, Pruessmann KP. k-t BLAST and k-t SENSE: Dynamic MRI With High Frame Rate Exploiting Spatiotemporal Correlations. Magn. Reson. Med. 2003; 50:1031–1042. [PubMed: 14587014]
38. Feng L, Axel L, Chandarana H, Block KT, Sodickson DK, Otazo R. XD-GRASP: Golden-angle radial MRI with reconstruction of extra motion-state dimensions using compressed sensing. Magn. Reson. Med. 2016; 75(2):775–88. [PubMed: 25809847]
39. McDonald RJ, McDonald JS, Kallmes DF, Jentoft ME, Murray DL, Thielen KR, Williamson EE, Eckel LJ. Intracranial Gadolinium Deposition after Contrast-enhanced MR Imaging. Radiology. 2015; 275(3):772–82. [PubMed: 25742194]
40. Malayeri AA, Brooks KM, Bryant LH, Evers R, Kumar P, Reich DS, Bluemke DA. National Institutes of Health Perspective on Reports of Gadolinium Deposition in the Brain. J. Am. Coll. Radiol. 2016; 13:237–41. [PubMed: 26810815]
41. Roberts DR, Lindhorst SM, Welsh CT, Maravilla KR, Herring MN, Braun KA, Thiers BH, Davis WC. High Levels of Gadolinium Deposition in the Skin of a Patient With Normal Renal Function. Invest. Radiol. 2016; 51:280–9. [PubMed: 26953564]

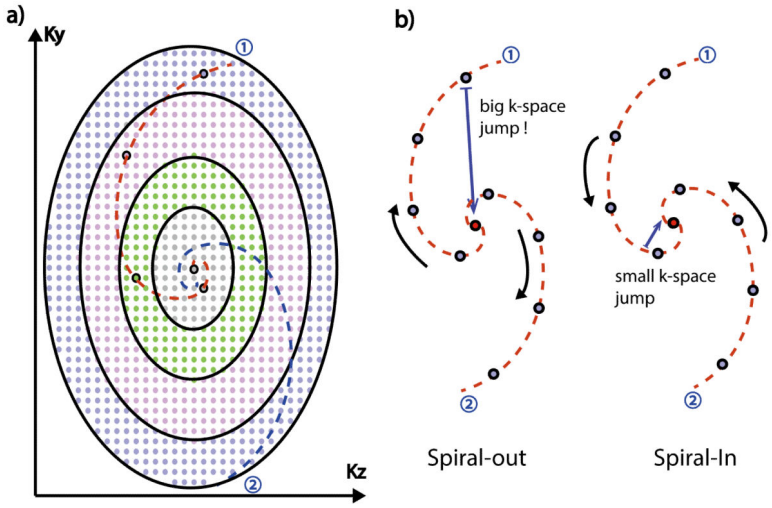

Figure 1.

Illustration of the ROCK sampling pattern (a). A “Spiral-In” trajectory was used in the ROCK to improve the quality of the self-gating signal by minimizing the k-space jump immediately preceding the acquisition of k-space center line.

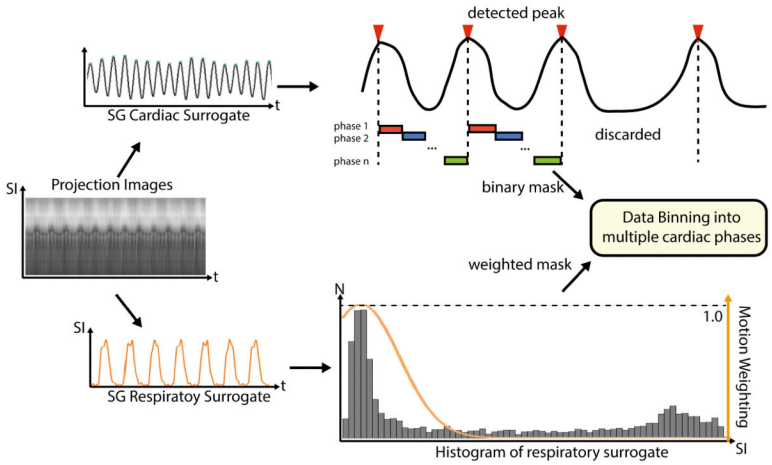

Figure 2.

K-space center-line are Fourier Transformed to SI projections, from which cardiac and respiratory SG signal was calculated. The amplitude of the respiratory SG signal was used to generate Gaussian weighted masks for respiratory motion soft-gating. K-space data was binned into multiple cardiac phases based on the cardiac triggers calculated by peak detection based on the cardiac SG signal.

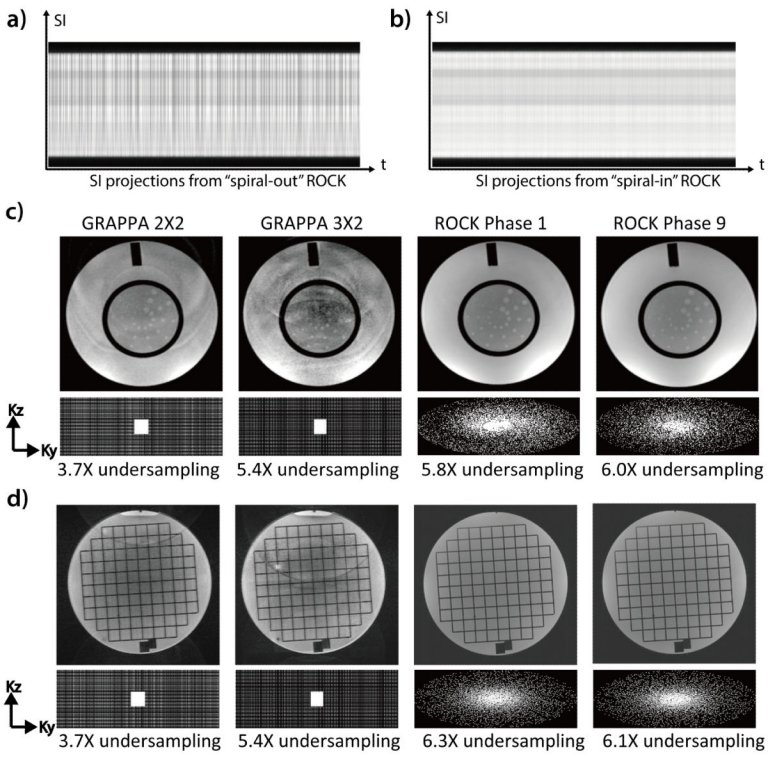

Figure 3.

The SI projections from the "spiral-out" ROCK (a) is subject to distortions due to eddy current artifacts and the same artifact is much alleviated in the "spiral-in" ROCK (b). Compared with images acquired using GRAPPA under-sampling, the images acquired using ROCK in 1.5T (c) and 3T (d) have better quality and less artifacts, though high under-sampling rates were achieved. In the ROCK method, the k-space after retrospective data binning has near-uniform angular distributions. The slightly different sampling pattern and under-sampling rate of different cardiac phases do not result in noticeable differences in image quality.

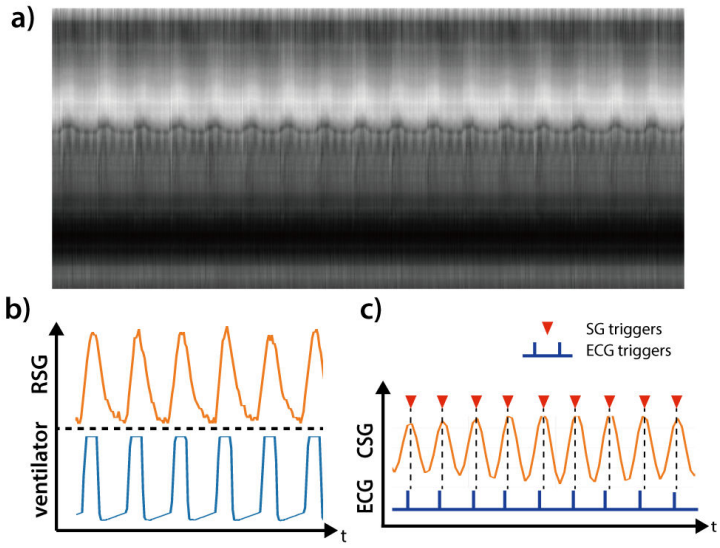

Figure 4.

The time series of SI projections on a 19 month old, male subject (a). The calculated respiratory self-gating (RSG) signal correlates well with the recorded airway pressure signal from mechanical ventilator (b). The calculated cardiac self-gating (CSG) trigger match with the recorded ECG triggers, albeit a small but near-constant delay.

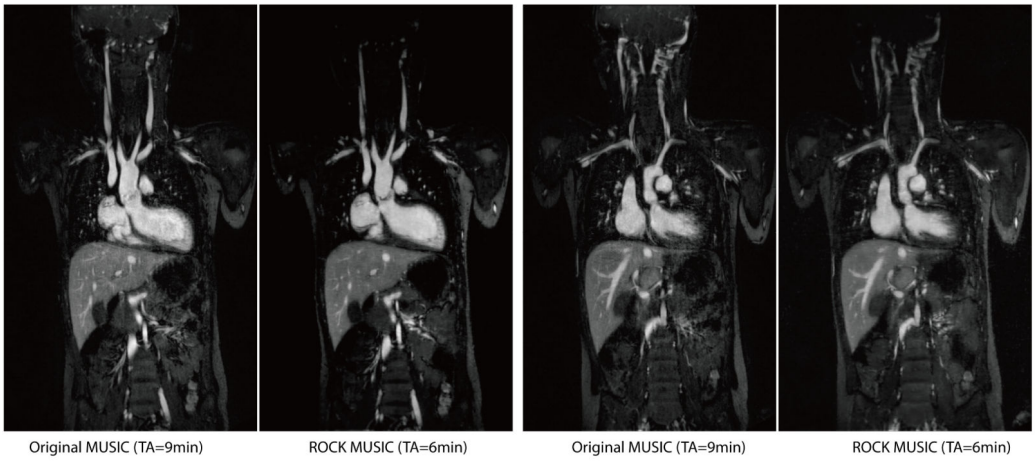

Figure 5.

Select images in cardiac systole and diastole from two full volume 4D studies of a 6 year old female patient. The ROCK-MUSIC images actually have slightly better image quality than the original MUSIC, but took 40% less time to acquire and were reconstructed without external physiological signals. All images are presented as single 1 mm partitions and were acquired with 1mm isotropic, non-interpolated resolution. The corresponding movies are available as Supporting Video S1 and S2.

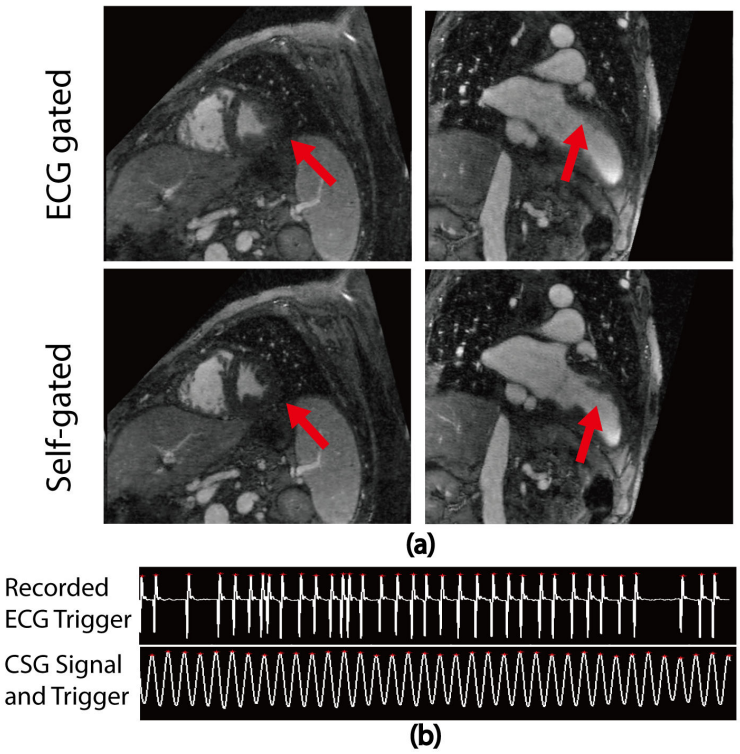

Figure 6.

Reconstructed images from an 8 year old male patient. The ROCK-MUSIC data were reconstructed separately using recorded ECG triggers and self-gating cardiac triggers (a). Regions that are subject to cardiac motion are blurred due to inaccurate triggering in the ECG-gated ROCK-MUSIC, but not in the self-gated ROCK-MUSIC, even though they are reconstructed based on the same dataset. The ECG signal in (b) are reconstructed signals based on recorded ECG-triggers. The real ECG-signal (not recorded) has severe distortions.

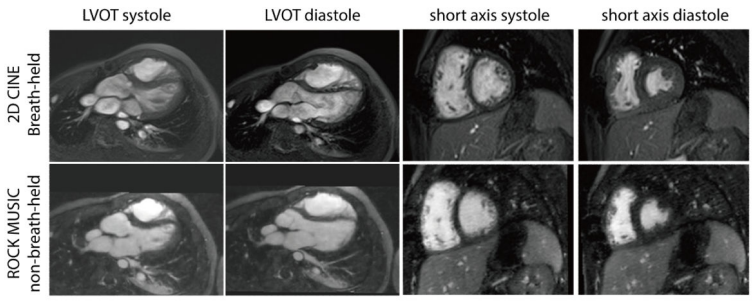

Figure 7.

The reformatted ROCK MUSIC has uniform blood-pool signal without in-flow effects typically seen on conventional 2D CINE. The blood-myocardium contrast is comparable even though a much thinner slice is used (5mm vs. 1mm). Some cardiac motion blur is visible in the systolic ROCK-MUSIC images due to the limited number of cardiac phases.

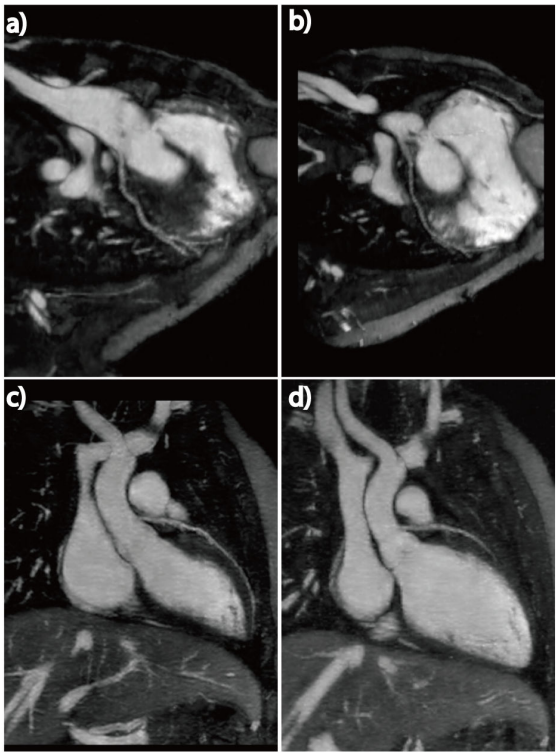

Figure 8.
The 4D nature of ROCK-MUSIC allows for clear reconstruction of large portions of the coronary arteries in multiple cardiac phases in this 8 year old male.

Table 1

SCORING CRITERIA

Aortic Root Pulmonary Arteries	1: non-diagnostic (vessels not visualized or diagnostically not assessable due to small size and /or motion artifact and /or poor contrast enhancement); 2: vessels visualized but with poor contrast enhancement and /or motion artifact so as to limit confident assessment and measurement of dimensions; 3: vessels visualized with good contrast so as to enable confident assessment of patency but with poor edge definition due to motion artifact so as to limit confident measurement of dimensions; 4: vessels visualized with good contrast and good edge definition such that patency and dimensions are confidently assessable
Ventricular outflow tracts (LVOT &RVOT)	1: non-diagnostic (structures not visualized or diagnostically not assessable due to small size and /or motion artifact and /or poor contrast enhancement; 2: annulus and sinotubular junction visualized but borders not sufficiently well defined for confident measurement; 3: annulus and sinotubular junction visualized with well-defined borders sufficient for confident measurement; 4: annulus and sinotubular junction clearly visualized with well-defined borders sufficient for confident measurement and leaflets seen
Cardiac Chambers	1: non-diagnostic (chambers not visualized or diagnostically not assessable due to small size and /or motion artifact and /or poor contrast enhancement; 2: chambers distinguishable but walls poorly defined, only gross features evaluable; 3: chambers clearly distinguishable with well-defined septum and free walls confidently evaluable but with poor definition of the papillary muscles and trabeculae; 4: chambers clearly distinguishable with excellent wall definition and with clear definition of the papillary muscles and trabeculae
Coronary Arteries	1: non-diagnostic (vessels not visualized or diagnostically not assessable due to small size and /or motion artifact and /or poor contrast enhancement); 2: only origins of main coronary arteries confidently identifiable; 3: origins and proximal course of RCA and left anterior descending (LAD) confidently evaluable; 4: origin, proximal and mid courses of RCA and LAD and proximal takeoff of left circumflex confidently evaluable

Table 2

SUBJECT IMAGE QUALITY SCORE

	Aortic Root Pulmonary Artery		Ventricular Outflow tracts		Cardiac Chambers		Coronary Arteries	
	Original MUSIC	ROCK-MUSIC	Original MUSIC	ROCK-MUSIC	Original MUSIC	ROCK-MUSIC	Original MUSIC	ROCK-MUSIC
Subject 1	3	4	3	4	3	4	2	4
Subject 2	3	4	3	4	3	4	3	4
Subject 3	4	4	3	4	3	4	4	4
Subject 4	2	4	2	4	3	4	2	2
Subject 5	3	4	3	4	4	4	4	3
Subject 6	3	4	3	4	3	4	3	4
Subject 7	4	4	4	4	4	4	3	4
Subject 8	3	4	3	4	3	4	3	4
Subject 9	4	3	4	3	4	3	4	3
Subject 10	4	4	3	4	3	4	2	4
Mean ± S.D.	3.3±0.67	3.9±0.32	3.1±0.57	3.9±0.32	3.3±0.48	3.9±0.32	3.0±0.82	3.6±0.70
P value	0.0759		0.033*		0.059		0.123	

* denotes statistical difference between original MUSIC and ROCK-MUSIC ($P<0.05$)